

A COST-EFFECTIVE PLANAR ELECTROMAGNETIC ENERGY HARVESTING TRANSDUCER

S. Roundy¹, E. Takahashi²

¹Department of Mechanical Engineering, University of Utah, Salt Lake City, USA

²EcoHarvester Inc., Berkeley, USA

Abstract: This paper presents a planar multi-pole electromagnetic energy harvesting transducer. We report on the design, manufacture, and performance results of integrated devices based on this transducer. The transducer leverages recent advancements in the manufacture of multi-pole magnets and can be implemented in a very cost effective manner using printed circuit board (PCB) technology. The basic transducer can be used for energy harvesting devices using a linear vibration or direct force input. This paper reports on a device that uses a direct force input that displaces the proof mass and then releases it, allowing it to freely oscillate. The device performance closely matches simulation and results in 11 mJ of generated energy and an efficiency of 9%.

Keywords: energy harvesting, electromagnetic, planar transducer

INTRODUCTION

Most motion based energy harvesting devices are implemented in a “blocky” form factor. For example, while piezoelectric sheets or bimorphs are thin, the motion required to generate energy is typically out-of-plane motion [1,2]. Electromagnetic generators often require magnets, coils, or proof masses that work best in a form factor that ends up looking like a cube or fat cylinder [3,4]. The goal of the work presented in this paper is to develop a very thin, planar electromagnetic energy harvesting transducer. Furthermore, the device presented here can be implemented with low cost materials and with a simple, low cost assembly process.

Several multi-pole magnetic generators have been reported in the literature [5,6]. The work presented here differs in at least two aspects: 1) it makes use of new manufacturing techniques enabling fine pitch multi-polar magnetic sheets that do not require assembly of multiple magnets in a housing [7], and 2) it uses a unique coil configuration to achieve a high generated voltage (greater than 3 volts) from linear oscillatory motion in a very thin form factor.

This paper will cover the basic operating principle, predictive modeling of the transducer, and simulation and experimental results.

OPERATING PRINCIPLE

As shown in Figure 1, the device consists of a PCB with planar coils, a multi-pole magnetic sheet, and springs which suspend the magnet over the PCB and maintain the gap between them. The magnet moves in the direction indicated in Figure 1. The mass can be driven by a direct force input, vibrations, or other inertial movements.

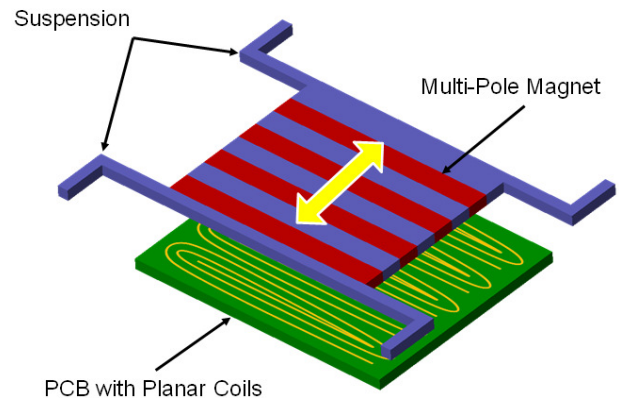


Figure 1. Schematic of basic transducer concept.

Figure 2 shows a 1 mm thick magnetic sheet with a pitch of 4mm. The illustration indicates the poling of the magnet, and the image shows the magnet itself. It is a NdFeB magnet manufactured for this application by Intermetallics Co. Ltd [7] using a proprietary process.

The magnet can be suspended above planar coils, which we call “serpentine” coils, as illustrated in Figure 1. In our case, the coils are implemented in a multi-layer PCB. The serpentine coil is illustrated in Figure 3. This configuration allows for multiple coils to be wired in series on each layer of the circuit board, and each layer to be wired in series with other layers resulting in a high voltage output. The prototype for which results are presented has 5 coils in series in each of 6 layers of the PCB. Other coil configurations are slightly more space efficient, but result in lower voltages (and higher currents), making the power electronics more complex.

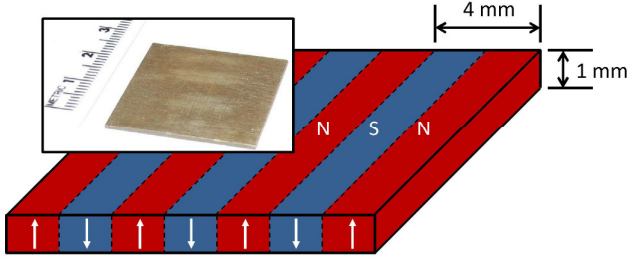


Figure 2. Illustration and image of the multi-pole plate magnet used for this work.

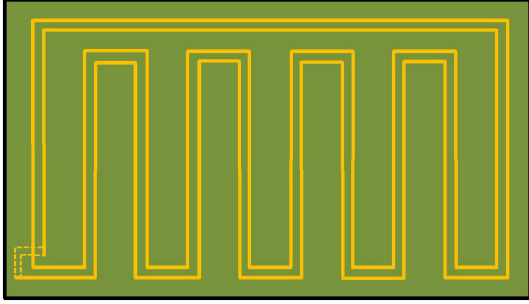


Figure 3. Illustration of planar coils on PCB. Two series coils shown. This pattern is repeated on each layer of the PCB.

THEORETICAL MODEL

A closed form simulation model has been developed based on electromagnetic theory which matches measured results well. Equations 1 through 3 describe the coupled electro mechanics of the system.

$$\frac{di}{dt} = -\frac{R+R_c}{L}i + \frac{1}{L}V_s \quad (1)$$

$$V_s = -\frac{d\Phi}{dt} = -Nl \frac{d}{dt} \left(\int_{x_1}^{x_2} B_y(x') dx' \right) \quad (2)$$

$$m\ddot{x} + b\dot{x} + N(\vec{i}l \times \vec{B}) + kx = F_{in}(t) \quad (3)$$

where:

- i - current through the coils
- R_c - coil resistance
- R - load resistance
- L - coil inductance
- V_s - generated open circuit voltage
- Φ - magnetic flux captured by coils
- N - number of coils
- l - length of one side of a rectangular coil
- B_y - magnetic flux density perpendicular to PCB
- x' - linear position on the PCB
- x - position of the magnet with respect to the PCB
- m - mass of the magnet
- b - mechanical damping coefficient
- k - stiffness of the flexures
- F_{in} - input force to the magnet

The solution to these equations is straightforward. However, each coil is in a different position with respect to the magnetic field. Therefore, the open circuit voltage (V_s) generated by each coil is slightly different both in magnitude and phase. Assuming that each coil generates the same voltage results in significant errors. One solution is to use finite element simulations to calculate the voltage generated by each individual coil. This, however, is cumbersome and not suitable for a predictive model to guide the design process. Therefore we developed an analytical description of the magnetic flux density (B_y) as a function of lateral position and distance from the magnet surface. This analytical description can be used to calculate the voltage contribution of each coil in an efficient way.

In order to use equation 2 for a numerical simulation, the shape of B_y must be known. We performed finite element simulations to determine the shape and strength of the magnetic field. Figure 4 shows the simulated magnetic flux with a steel pole piece placed behind the magnet. Figure 5 shows the simulated magnetic flux density (B_y) at various distances from the magnet. Note that point measurements were made with a gaussmeter to validate the finite element simulations. Looking at Figure 5, the assumption that $B_y(x')$ is sinusoidal is fairly good as long as coil is at least 0.2 mm away from the surface. Even in cases where the coil is slightly closer, the sinusoidal assumption results in negligible errors. Fitting the data from these simulations results in the expression in equation 4, which approximates the magnetic flux density as a function of lateral position and distance from the magnet surface.

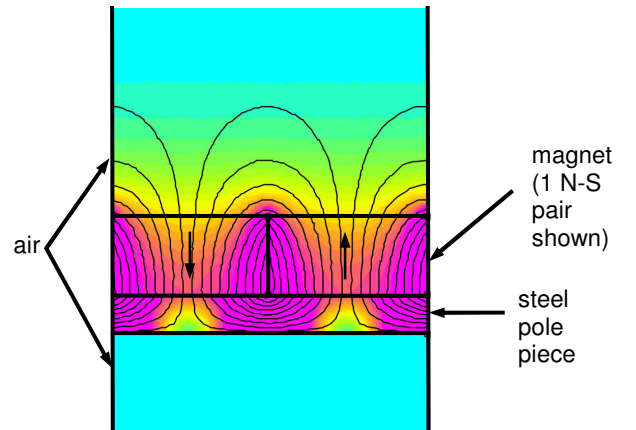


Figure 4. 2-D finite element simulation results for magnetic field. A steel pole piece is placed behind the magnet. A PCB with coils is placed in the air gap above the magnet.

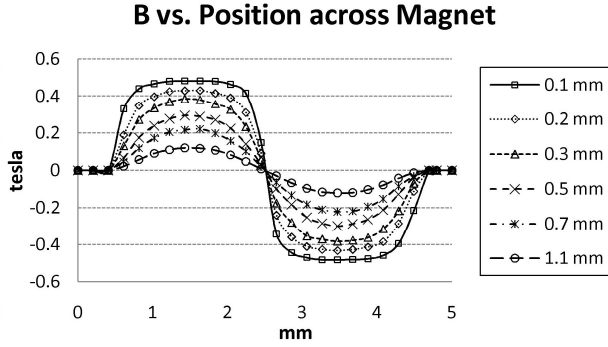


Figure 5. Finite element simulation results. Magnetic flux density perpendicular to the magnet at various distances shown for one pair of magnetic poles (1 pitch).

$$B_y(x') = B_{\max} e^{-\alpha y(i)} \sin\left(\frac{2\pi}{p}(x' - x(t))\right) \quad (4)$$

where:

- B_{\max} – maximum value of $B_y(x')$ at the magnet surface
- $y(i)$ – distance from magnet surface of the i^{th} PCB layer
- α – empirically generated coefficient
- p – magnet pitch

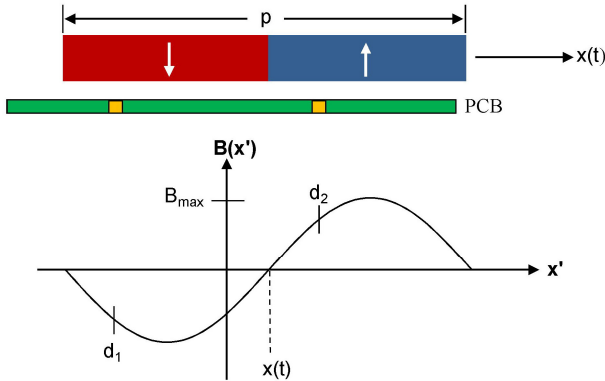


Figure 6. Magnetic flux density approximation and definition of variables.

Using equation 4, a closed form expression for the magnetic flux (Φ) captured by each coil can be developed. However, we first need to note a subtlety relating to the position variables x' and $x(t)$. Figure 6 shows two poles of the magnet, a cross section of the PCB, and the assumed shape of $B(x')$. x' is the position on the PCB. d_1 and d_2 mark the positions of the metal lines of a single rectangular coil on the $B(x')$ curve. $x(t)$ is the position of the magnet relative to the PCB, and is moving in time. So, the whole sinusoid is moving back and forth along x' , but the d_1 and d_2 locations are stationary. Substituting equation 4 into equation 2, and performing the integration results in the expressions in equations 5 and 6 for Φ and $d\Phi/dt$.

These equations form the basis for efficient numerical simulation and guide the design process.

$$\Phi = \frac{-NIB_{\max} e^{-\alpha y(i)} p}{2\pi} \left\{ \left[\sin\left(\frac{2\pi d_2}{p}\right) - \sin\left(\frac{2\pi d_1}{p}\right) \right] \sin\left(\frac{2\pi}{p} x(t)\right) + \left[\cos\left(\frac{2\pi d_2}{p}\right) - \cos\left(\frac{2\pi d_1}{p}\right) \right] \cos\left(\frac{2\pi}{p} x(t)\right) \right\} \quad (5)$$

$$\frac{d\Phi}{dt} = -NIB_{\max} e^{-\alpha y(i)} \dot{x} \left\{ \left[\sin\left(\frac{2\pi d_2}{p}\right) - \sin\left(\frac{2\pi d_1}{p}\right) \right] \cos\left(\frac{2\pi}{p} x(t)\right) - \left[\cos\left(\frac{2\pi d_2}{p}\right) - \cos\left(\frac{2\pi d_1}{p}\right) \right] \sin\left(\frac{2\pi}{p} x(t)\right) \right\} \quad (6)$$

This model has proven very accurate and can therefore be used as a basis for design optimization within the constraints of a given application.

RESULTS

Several prototypes have been built based on this technology, one of which is shown in Figure 7. Note that in this case, the PCB and magnet have been switched so that the PCB moves and the magnet is stationary. This prototype is intended for direct force input. As such, the proof mass is displaced with a force of 12 N, which results in a 2 mm displacement, and released. The voltage was measured across a 20 Ω resistor. The measured and simulated voltage response is shown in Figure 8. The generated energy is 1.1 mJ from 12 mJ of input energy resulting in an efficiency of 9%. The generator has also been used to charge a capacitor powering a wireless transceiver which can transmit 3 independent data packets from a single actuation cycle. Figure 9 shows the voltage across the storage capacitor and the combined current draw of the microprocessor and radio. The system turns on at about 5 mSec. The three data transmissions are clearly visible as the 25 – 30 μ A pulses.

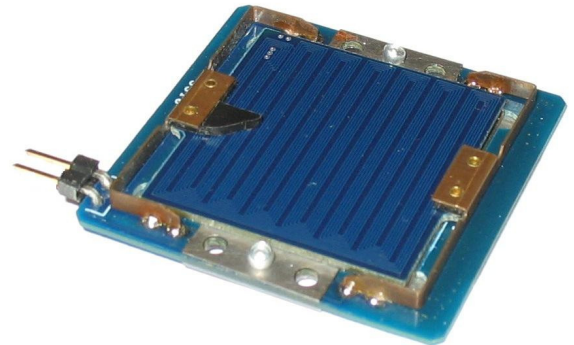


Figure 7. Prototype generator. Size is approximately 37 X 37 X 3 mm. Magnet plate is underneath the PCB. PCB is the proof mass.

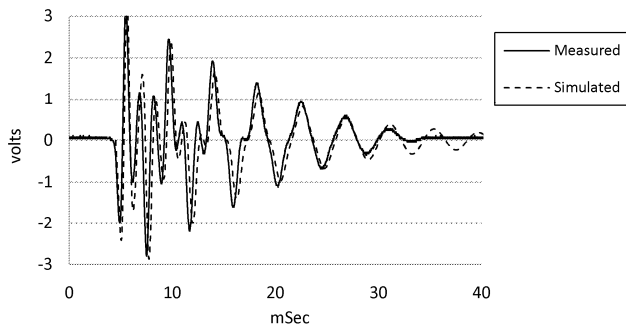


Figure 8. Measured and simulated output voltage across a 20Ω load resistor from an initial displacement of 2 mm.

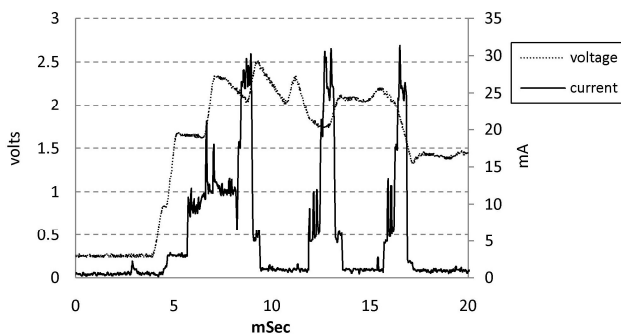


Figure 9. Voltage across a $60 \mu\text{F}$ storage capacitor and current draw demonstrating 3 data transmission packets for a single actuation.

DISCUSSION

Note in Figure 8 that there are two frequencies present in the voltage signal. The lower frequency is the mechanical oscillation of the proof mass. The higher frequency is due to the pitch of the magnets. At first, the mechanical amplitude is high, and the PCB passes over multiple magnetic transitions in a single mechanical oscillation. As the oscillation dies down, the PCB does not cross over multiple magnet boundaries, and so the only frequency visible is the oscillation of the proof mass.

The power output is very sensitive to both the air gap between the PCB and the magnet and the mechanical damping ratio. The air gap is closely controlled during the assembly process. The damping ratio of the device is measured and then fed back into the simulation. With these two numbers either measured or controlled accurately, the model has excellent predictive capability.

The PCB shown in Figure 7 has six layers. The coils on the layer closest to the magnet are the most productive in that they generate a higher voltage than the coils on the layer furthest away from the magnet. Of course, each coil contributes the same resistance,

so adding extra layers to the PCB has diminishing returns.

The prototype shown in Figure 7 uses the PCB as the moving proof mass and the magnets are stationary. This lower mass increases the velocity of the proof mass for given energy input (12 mJ in this case). The increased velocity results in a higher generated voltage. Note that the higher generated voltage does not translate to more total energy being generated per actuation cycle. A larger proof mass will generate the same amount of energy, but at over a longer period of time and at lower peak voltages. As a higher voltage reduces the other constraints on the system, we used the lower mass PCB as the moving element.

CONCLUSIONS

We have presented a planar linear energy harvesting transducer. The transducer can be used for devices that generate power from either a direct force input or from vibrations. We have demonstrated a generator powered by a direct force input. The generator employs novel manufacturing techniques to realize a thin multi-pole magnet and a novel coil configuration implemented in a multi-layer PCB. The measured results match theoretical modeling very closely. Finally, we have used the device to power a wireless system in which 3 data packets have been transmitted from a single actuation cycle.

REFERENCES

- [1] Lefeuvre E., Badel A., Richard C., Guyomar D. 2005 Piezoelectric Energy Harvesting Device Optimization by Synchronous Electric Charge Extraction. *J. Intel. Mat. Syst. Str.*, **16**(10), 865-876.
- [2] Roundy S., Wright P. K. 2004 A piezoelectric vibration based generator for wireless electronics. *Smart Mater. Struct.*, **13**(5), 1131-1142.
- [3] Torah R., Glynn-Jones P., Tudor, M., O'Donnell T., Roy S., Beeby, S. 2008 Self-powered autonomous wireless sensor node using vibration energy harvesting. *Meas. Sci. Technol.*, **19**(12), 125202.
- [4] Perpetuum Ltd., "PMG FSH Free Standing Harvester Datasheet," PMG FSH Technical Datasheet, May 2010.
- [5] Arnold D.P., 2007 Review of Microscale Magnetic Power Generation. *IEEE T Magn.*, **43**(11), 3940-3951.
- [6] Trimble A.Z., Lang J.H., Pabon J., Slocum A. 2010 A Device for Harvesting Energy From Rotational Vibrations. *J. Mech. Design*, vol. 132, (2010) 091001.
- [7] Sagaway M., Mizoguchi T., Asazuma M., Hayashi S. 2012 Method and System for Producing Sintered NdFeB Magnet, and Sintered NdFeB Magnet Produced by the Production Method. *US Patent Pub. No. 2012/0176212 A1*.